Rest Frame Interference in Rotating Structures and Metamaterials

Y. Mazor and Ben Z. Steinberg

Phys. Rev. Lett. **123**, 243204 — Published 13 December 2019

DOI: 10.1103/PhysRevLett.123.243204

Rest frame interference in rotating structures and metamaterials

Y. Mazor and Ben Z. Steinberg
School of EE, Tel-Aviv University
(Dated: November 14, 2019)

Using the formulation of electrodynamics in rotating media, we put into explicit quantitative form the effect of rotation on interference and diffraction patterns as observed in the rotating medium's rest-frame. As a paradigm experiment we focus the interference generated by a linear array of sources in a homogeneous medium. The interference is distorted due to rotation; the maxima now follow curved trajectories. Unlike the classical Sagnac effect in which the rotation induced phase is independent of the refraction index n, here the maxima bending increases when n decreases, suggesting that ϵ-near-zero metamaterials can enhance optical gyroscopes and rotation-induced non-reciprocal devices. This result is counter intuitive as one may expect that a wave that travels faster would bend less. The apparent contradiction is clarified via the Minkowski momentum picture for a quasi-particle model of the interference that introduces the action of a Coriolis force, and by the Abraham picture of the wave-only momentum. our results may also shed light on the Abraham-Minkowski controversy as examined in non-inertial electrodynamics.

Introduction Non-reciprocal electrodynamics finds diverse applications in technology and engineering. It constitutes the basis for devices such as one-way waveguides, circulators, and isolators, that are important components in functional electromagnetic and acoustic systems. Three types of schemes have been suggested for breaching reciprocity [1]. (i) Magnetic biasing and the magneto-optic effect [2, 3]. (ii) Medium nonlinearity [4, 5]. (iii) Spatio-temporal variation of material properties or its rotation [6–12]. In all of these schemes, interest is focused on the electrodynamic phenomena as observed in the laboratory (inertial) Frame of Reference (FoR).

Non-reciprocity based on rotating media is important not only for the devices mentioned above; it plays a pivotal role in rotation sensors and optical gyroscopes. Here, interest is focused on observing the device's electrodynamics in the rotating structure *rest* FoR, $\mathcal{R}^\Omega$, that is non-inertial. This is motivated by the use of gyroscopes for independent navigation systems. Their operation is mainly based on the Sagnac effect - manifestation of non-reciprocity of a rotating medium as observed in its rest frame [13–16]. These applications have motivated studies of rotating Photonic Crystals [17, 18], guiding structures [19–21], mode degeneracy in rotating cavities [18, 22], and rotating open cavities [23, 24], to name a few. Analysis of rigidly rotating structures in $\mathcal{R}^\Omega$ also offers significant advantages by avoiding the need to deal with moving boundaries (albeit at the expense of more complicated constitutive relations [25, 26]). Numerical solvers based on FDTD approach that explicitly use this advantage were also developed [28, 29]. Thus, even if the final results of interest are fields observed in the laboratory inertial FoR, one may be better off solving the electrodynamic problem in $\mathcal{R}^\Omega$, and then apply field transformations [30, 31]. Therefore, this approach may prove suitable to study rigidly rotating complex structures such as metamaterials and metasurfaces, and may lead to a new realm of applications for optical gyroscopes and other non-reciprocal devices.

In this work we study the effect of slow rotation on the interference generated by electrically small and equally excited scatterers embedded in a rigidly rotating material with constant angular velocity $\mathbf{\Omega}$. We explore the rotation footprint on the interference pattern observed at the structure's rest FoR $\mathcal{R}^\Omega$, and show that the Interference Maxima (IM) follow curved trajectories, whose curvature depends on Ω. While this result by itself is intuitive, there are two new fundamental observations about the rotation footprint. First, unlike the Sagnac effect which is medium-independent [13, 15, 16], here the bending of the IM depends on the medium refraction index n. Second, the bending *increases* as n *decreases*. The last observation is counter-intuitive: one would expect that if the wave travels faster for a given Ω, its bending would decrease. We resolve the apparent contradiction by using, respectively, the Abraham and Minkowski pictures for the energy and momentum of the associated wave and quasi-particle interpretations of the interference pattern. Clearly, the fact that the rotation footprint on interference increases as n decreases is a fundamentally new result that calls for novel applications of metamaterials and near-zero index materials in optical gyroscopes and other rotation based non-reciprocal devices.

Formulation We *define* $\mathcal{R}_I$ as a static inertial FoR, in which the basic physical laws appear in their simple familiar form; space-time is flat

(gravitation neglected, and Riemann curvature vanishes) hence the system geometry is locally *Lorentzian* [27], and Maxwells equations take on their familiar form in vacuum within the framework of special relativity. A stationary material present in this system is represented here by the scalars $\epsilon(\boldsymbol{r}), \mu(\boldsymbol{r})$.

We study an interference experiment in materials and structures that rotate rigidly at a constant angular velocity $\boldsymbol{\Omega} = \Omega\hat{\boldsymbol{z}}$ with respect to $\mathcal{R}_I$. The spatial extent d normal to $\hat{\boldsymbol{z}}$ occupied by the material is finite, and the rotation is slow such that $\Omega d \ll c$. Since the system is Lorentzian, one may define this rotation with respect to $\mathcal{R}_I$ in the naïve way: follow a specific atom, measure the time interval Δt until it accomplishes a complete round, then set $\Omega = 2\pi/\Delta t$. We focus on the Electrodynamics (ED) as seen by an observer that is *fixed* to the rotating material/structure. Hence we define the rotating FoR $\mathcal{R}^\Omega$. This is the *appropriate reference frame* [27]: it is at rest relative to all apparatus, sensors, etc., that are bolted to the material. Here and henceforth, we always observe the ED as seen in the (always) appropriate FoR $\mathcal{R}^\Omega$, and the corresponding ED problem is termed as the "$\mathcal{R}^\Omega$ problem". The specific case of $\mathcal{R}^0$ and "$\mathcal{R}^0$ problem" corresponds to $\Omega = 0$, meaning that the material and the observer appear at rest in the inertial FoR $\mathcal{R}_I$, rendering $\mathcal{R}^0$ and $\mathcal{R}_I$ the same.

$\mathcal{R}^\Omega$, $\Omega \neq 0$ is non-inertial; an observer at rest there sees curved space-time. However, space-time in $\mathcal{R}^\Omega$ can be considered *locally flat* (and Lorentzian) for distances D satisfying [27],

$$D \ll L = c^2/A, \tag{1}$$

where A is the acceleration of $\mathcal{R}^\Omega$. In our case $A = \Omega^2 D$, so Eq. (1) yields *precisely* the slow rotation condition mentioned above, $\Omega D \ll c$. Our work is limited to this domain of space-time flatness.

Our analysis is two-dimensional; the scatterers geometry and electromagnetic excitations are invariant along $\hat{\boldsymbol{z}}$ - the rotation axis. Thus, point sources and point scatterers are 2D in nature and represent thin wires extended along the z-axis, as in [32]. The reader is referred to [33] for a discussion of possible 3D realizations, and the underlying physical principles and limitations. Vectors are in bold letters, and a hat indicates unit-vectors. In $\mathcal{R}^\Omega$ the coordinates normal to the rotation axis $\hat{\boldsymbol{z}}$ are $\boldsymbol{\rho} = \hat{\boldsymbol{x}}x + \hat{\boldsymbol{y}}y = \rho\hat{\boldsymbol{\rho}}$. We assume that the materials in the corresponding $\mathcal{R}^0$ problem are characterized by scalar permittivity $\epsilon = \epsilon_0\epsilon_r$ and permeability $\mu = \mu_0\mu_r$. The corresponding speed of light in vacuum and refraction index for $\mathcal{R}^0$ problem are $c = 1/\sqrt{\epsilon_0\mu_0}$ and $n = \sqrt{\epsilon_r\mu_r}$, respectively. The covariant formulation of electrodynamics of a slowly rotating medium, for $\mathcal{R}^\Omega$ problem, is given by the same set of Maxwell equations as for the stationary case with modified constitutive relations to account for the rotation effect [25, 26]. Our starting point is the Green's function theory developed in [32]. It has been shown that in 2D problems the electromagnetic field can be rigorously separated into completely decoupled TE and TM polarizations comprising of $(Hz, \boldsymbol{E}_t)$ and $(Ez, \boldsymbol{H}_t)$ fields, respectively. An exact Green's function expression has been derived, from which *all* the field components can be uniquely extracted. Relevant results are summarized in [33], including a formally exact representation in terms of cylindrical harmonics summation (e.g. Eq. (5a)). Under the slow rotation assumption $\max(\rho, \rho')\Omega/c \ll 1$ this Green's function is

$$G(\boldsymbol{\rho}, \boldsymbol{\rho'}) \simeq G^{\text{st}}(\boldsymbol{\rho}, \boldsymbol{\rho'}) e^{ik_0(\Omega/c)\hat{\boldsymbol{z}}\cdot(\boldsymbol{\rho'}\times\boldsymbol{\rho})}, \tag{2}$$

where G^{st} is the homogeneous medium Greens function for $\mathcal{R}^0$ problem, $G^{\text{st}}(\boldsymbol{\rho}, \boldsymbol{\rho'}) = \frac{i}{4}H_0^{(1)}(k_0 n|\boldsymbol{\rho} - \boldsymbol{\rho'}|)$, and $H_0^{(1)}$ is the Hankel function of the first kind.

Up to a multiplication constant, H_z and E_z in the TE and TM polarizations, respectively, are given by this Green's function. Unlike the infinite summation over cylindrical harmonics, this approximation explicitly incorporates the physically meaningful entities of amplitude, phase, and optical path [32]. Since c is the speed of light in vacuum, for $\mathcal{R}^0$ problem, the rotation footprint is manifested only in the exponential term, and is *independent* of the medium refraction index n.

Reconstruction of the Sagnac effect It has been shown in [32] that the full expression for G (Eq. (5a) in [33]) contains the entire electrodynamic spectrum of a rotating medium, from which the Sagnac effect can be derived. The following simple analysis shows that the Sagnac phase shift is faithfully represented in Eq. (2).

Consider the set of N point-scatterers shown in Fig. 1. Assume that scatterer #1 is excited by a unit field, and follow the wave-field that hits and excites scatterer #2, then #3 etc..., until it completes a closed loop. Since all scatterers are electrically small, their excitation can be faithfully described by the associated polarizabilities $\alpha_n, n = 1, \ldots N$ and induced dipole moments $p_n = \alpha_n E^L(\boldsymbol{\rho}_n)$, where $E^L(\boldsymbol{\rho}_n)$ is the local field at the n-th scatterer center: the field there, in the absence of that specific scatterer. Hence, at the completion of the loop the field

is

$$E = \Pi_{m=1}^{N} \alpha_m G(\boldsymbol{\rho}_m, \boldsymbol{\rho}_{m-1}) \tag{3}$$

where we set $\boldsymbol{\rho}_0 \equiv \boldsymbol{\rho}_N$. Rewriting this using Eq. (2), we get

$$E = \left[\Pi_{m=1}^{N} \alpha_m G^{\rm st}(\boldsymbol{\rho}_m, \boldsymbol{\rho}_{m-1})\right] e^{i\phi}. \tag{4a}$$

The expression in the square brackets is the field after it accomplishes a complete loop in a $\mathcal{R}^0$ problem, which includes the effect of the refraction index n. Since the footprint of rotation on the scatterers' polarizabilities is negligible [34], it manifests only in ϕ,

$$\phi = 2k_0 \frac{\Omega}{c} \sum_{m=1}^{N} S_{\triangle_m} = 2k_0 \frac{\Omega}{c} S, \tag{4b}$$

where $S_{\triangle_m} = \hat{\boldsymbol{z}} \cdot (\boldsymbol{\rho}_{m-1} \times \boldsymbol{\rho}_m)/2$ is the *area* of the triangle whose vertices are the origin (=rotation axis) and $\boldsymbol{\rho}_{m-1}, \boldsymbol{\rho}_m$. $S \equiv \sum_m S_{\triangle_m}$ is the total area enclosed by the loop, and it follows that ϕ is *independent* of the refraction index n of the surrounding medium. This result is nothing but the celebrated Sagnac phase-shift [13]. Also, we note that the total area enclosed by the loop becomes negative if the series of events is inverted (representing propagation in the opposite direction). This fact establishes the well known Sagnac phase shift $\Delta\phi = 4k_0\Omega|S|/c$ between clockwise and counter clockwise propagating waves. Finally, it is straightforward to show that these results hold also if the rotation axis is outside the closed loop.

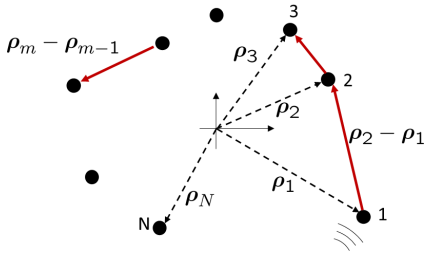

FIG. 1. N scatterers forming a Sagnac loop of scattering events. The structure rotates around the origin at angular velocity $\boldsymbol{\Omega} = \hat{\boldsymbol{z}}\Omega$, and is observed at $\mathcal{R}^{\Omega}$.

The purpose of the analysis above is to verify that the Sagnac phase shift is correctly preserved in the approximation; this is important since it enables us to use a simple and physically transparent expression for G (and consequently for the phases) in subsequent derivations. Furthermore, the new results below seem to contradict Sagnac effect, but this apparent contradiction is derived using the same Green's function that correctly reconstructs Sagnac effect, and therefore they are mathematically consistent.

A paradigm interference experiment Consider an infinite linear periodic array of point scatterers shown in Fig. 2, observed in $\mathcal{R}^{\Omega}$. For simplicity, we assume an identical excitation magnitude of all scatterers, and examine the interference pattern of the system in the far-field. Being electrically small, the radiation of the m-th scatterer is given by $G(\boldsymbol{\rho}, \boldsymbol{\rho}'_m)$ where $\boldsymbol{\rho}'_m$ is its location,

$$\boldsymbol{\rho}'_m = \boldsymbol{\rho}'_0 + m\boldsymbol{d} = \boldsymbol{\rho}'_0 + md\hat{\boldsymbol{d}}, \tag{5}$$

$\boldsymbol{d} = d\hat{\boldsymbol{d}}$ is the array lattice vector, and d is the period length. The interference field at an arbitrary observation point $\boldsymbol{\rho}$ is [use Eq. (2)]

$$E(\boldsymbol{\rho}) = \sum_m G(\boldsymbol{\rho}, \boldsymbol{\rho}'_m) \tag{6a}$$

$$= \sum_m G^{\rm st}(\boldsymbol{\rho}, \boldsymbol{\rho}'_m) e^{ik_0 \frac{\Omega}{c} \hat{\boldsymbol{z}} \cdot (\boldsymbol{\rho}'_m \times \boldsymbol{\rho})}. \tag{6b}$$

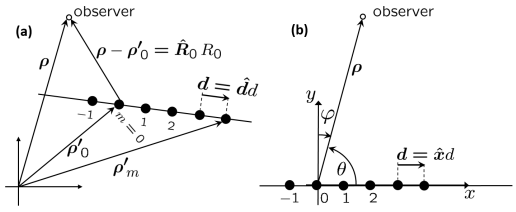

FIG. 2. A periodic array of point-scatterers. (a) The general setting. (b) The effect of rotation is maximized in regions where $\boldsymbol{\rho} \perp \hat{\boldsymbol{d}}$.

We invoke now the standard algebraic procedure used to obtain the far-field. First, use the large argument approximation of $H_0^{(1)}$ in $G^{\rm st}$: $H_0^{(1)}(x) \simeq \sqrt{2/(\pi x)} e^{i(x-\pi/4)}$. In the amplitude we approximate $1/|\boldsymbol{\rho} - \boldsymbol{\rho}'_m| \simeq 1/R_0 \; \forall m$, where $R_0 = |\boldsymbol{\rho} - \boldsymbol{\rho}'_0|$. In the exponent we set $|\boldsymbol{\rho} - \boldsymbol{\rho}'_m| \simeq R_0 - m\boldsymbol{d} \cdot \hat{\boldsymbol{R}}_0$ where $\hat{\boldsymbol{R}}_0$ is a unit vector defined by $\hat{\boldsymbol{R}}_0 = (\boldsymbol{\rho} - \boldsymbol{\rho}'_0)/R_0$. Substituting it back to Eq. (6b) we get with no further approximation

$$E \simeq \frac{e^{i\pi/4} e^{ik_0\left[nR_0 - \frac{\Omega}{c}\hat{\boldsymbol{z}} \cdot (\boldsymbol{\rho} \times \boldsymbol{\rho}'_0)\right]}}{(8\pi k_0 n R_0)^{1/2}} \sum_{m'} e^{-im'q}, \tag{7a}$$

where

$$q = k_0 d \left[n\hat{\boldsymbol{d}} \cdot \hat{\boldsymbol{R}}_0 + \frac{\Omega}{c} \hat{\boldsymbol{z}} \cdot (\boldsymbol{\rho} \times \hat{\boldsymbol{d}})\right]. \tag{7b}$$

Clearly, the field in Eq. (7a) peaks when q becomes an integer multiple of 2π. Therefore

the IM are obtained at $\boldsymbol{\rho} = \boldsymbol{\rho}_{\mathfrak{M}}$ given by ($\mathfrak{M} = 0, \pm 1, \pm 2, \ldots$)

$$n\hat{\boldsymbol{d}} \cdot \hat{\boldsymbol{R}}_0^{\mathfrak{M}} + \frac{\Omega}{c}\hat{\boldsymbol{z}} \cdot (\boldsymbol{\rho}_{\mathfrak{M}} \times \hat{\boldsymbol{d}}) = \mathfrak{M}\frac{\lambda}{d}, \qquad (8)$$

with $\hat{\boldsymbol{R}}_0^{\mathfrak{M}} \equiv (\boldsymbol{\rho}_{\mathfrak{M}} - \boldsymbol{\rho}_0')/\left|\boldsymbol{\rho}_{\mathfrak{M}} - \boldsymbol{\rho}_0'\right|$, and λ is the vacuum wavelength in $\mathcal{R}^0$. The rotation footprint is most profound where $\boldsymbol{\rho} \perp \hat{\boldsymbol{d}}$. In these regions the specific choice of $\boldsymbol{\rho}_0$ has no significant role, so one may conveniently set $\boldsymbol{\rho}_0 = \boldsymbol{0}$ as illustrated in Fig. 2(b). Assume now we observe the interference on a screen parallel to the array axis, located at a constant range $y > 0$. We define $\varphi_{\mathfrak{M}} = \pi/2 - \theta_{\mathfrak{M}}$ as the angle between the y axis and $\boldsymbol{\rho}_{\mathfrak{M}}$ ($-\pi/2 < \varphi_{\mathfrak{M}} < \pi/2$). Then, for the specific setting in Fig. 2(b) the general expression in Eq. (8) yields [33]

$$\varphi_{\mathfrak{M}} = \arcsin\left[\frac{1}{n}\left(\frac{\mathfrak{M}\lambda}{d} + \frac{\Omega y}{c}\right)\right]. \qquad (9)$$

For $\Omega = 0$ it produces the traditional result of diffraction grating in $\mathcal{R}^0$. Rotation adds a *range-dependent* term, making the IM follow *curved trajectories* in space with bending that depends on n. This is to contrast with the classical Sagnac effect, reconstructed above, that is *medium independent*. The bending scales as n^{-1}, and it exists already at the zeroth-order diffraction term ($\mathfrak{M} = 0$). Therefore low-index enhances sensitivity to rotation. This enhancement, however, is not unbounded since n has a lower bound: $n > \frac{\mathfrak{M}\lambda}{d} + \frac{\Omega y}{c}$ to render $\varphi_{\mathfrak{M}}$ real. For $\mathfrak{M} = 0$ it yields $n > \Omega y/c$. For example assume $\Omega \approx 7.3 \times 10^{-5}$ sec^{-1} (earth rotation). For $y = 1$m, $n > 2.4 \times 10^{-13}$. Hence one can get enhancement of many orders of magnitude before the lower bound on n is approached. As Ω gets smaller, so does the lower bound on n, thus enabling a stronger enhancement of sensitivity to rotation.

We computed the interference field by using Eq. (6a) with the exact Green's function in Eq. (5) in [33] (G_{exact}), and with the simplified expression in Eq. (2). The system consists of eight points located at $y_m = 0$ and $x_m = \lambda[-14, -10, -6, -2, 2, 6, 10, 14]$, where λ is the vacuum wavelength, and the background is vacuum. The results are shown in Figs. 3(a)-(c) for $\Omega/\omega = 3 \times 10^{-5}$. The x, y coordinates are in units of λ. Figure 3(a) shows the interference as obtained from Eq. (6a) with G_{exact} with $\ell = -80, ..., 80$. Figure 3(b) shows the same but with $\ell = -160, ..., 160$. It is seen that the patterns carry the same physical picture of curved IM, but differ in some details. Figure 3(c) shows the interference computed with the approximate Green's function in Eq. (6a). It is identical to Fig. 3(b). In all cases, the IM follow the curved trajectories predicted by Eq. (9).

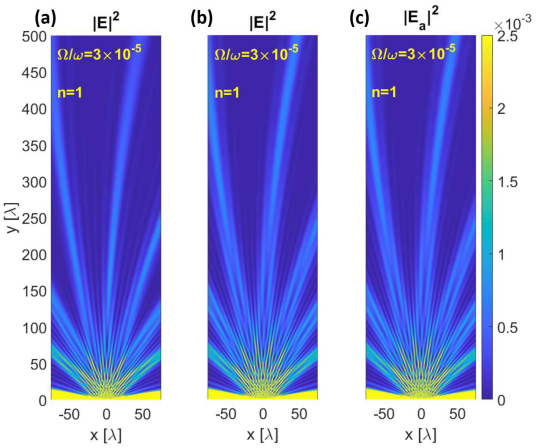

FIG. 3. Interference patterns due to eight point-scatterers. (a) Using Eq. (6a) with the formal expansion in Eq. (5) of [33] for G with 161 cylindrical harmonics. (b) With 321 cylindrical harmonics. (c) Using the G in Eq. (2). Coordinates are normalized to the vacuum wavelength. The axes and colormaps are the same for all sub-figures. The IM match Eq. (9).

Figure 4 shows the interference of the same system as in Fig. 3, but now the background refraction index is $n = 0.5$. The IM bending increased significantly, and matches Eq. (9). This last observation is counter intuitive. Lower n implies faster wave, and one would expect a faster wave to bend *less*, while Eq. (9) predicts the contrary. We clarify this apparent contradiction below.

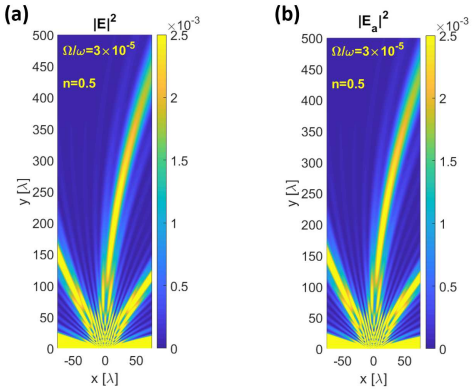

FIG. 4. The same as in Fig. 3, but with a background medium with refraction index $n = 0.5$. (a) With G in Eq. (5) of [33] and 321 cylindrical harmonics. (b) Using G of Eq. (2). Bending of the IM increased according to Eq. (9).

Finally, we note that the Fresnel drag coeffi-

cient (or Fizeau drag) [35] $\alpha = 1-n^{-1}$ measures the degree of non-reciprocity of light propagation in moving medium in the inertial frame, and it has been related to the space-time metric. Low n may invert the drag direction, and even the metric sign. This intriguing observation needs to be clarified by further study.

Energy and momentum pictures The time-averaged power flux and momentum densities associated with the wave *only*, in non-inertial frame, are still given by $\boldsymbol{S} = \frac{1}{2}\Re(\boldsymbol{E} \times \boldsymbol{H}^*)$ and by $\boldsymbol{S}/c^2$, respectively [36]. The latter is nothing but the Abraham momentum picture [36, 37]. $\boldsymbol{S}$ for a line source of electric current is given by Eqs. (11a)-(11e) in [33], which includes [38] for further analogy. For $\rho'/\rho \to 0$ we have $S_\rho \propto n$ and Ω-independent, while $S_\theta \propto \Omega$ and has n-independent magnitude. Thus the *ratio* S_θ/S_ρ increases as n decreases, which results in stronger bending. We note that in the Minkowski picture the momentum density is $\frac{1}{2}\Re(\boldsymbol{P} = \boldsymbol{D} \times \boldsymbol{B}^*)$. This expression, however, does not distinguish between the wave and medium parts and therefore it is less convenient for exposing the mechanism underlying the effect of n on the field interference bending.

Since the curved IM in Eq. (9) and Figs. (3)-(4) are due to interference, a better description that is consistent with the Minkowski picture *and* takes into account the medium effect, is based on a *quasi-particle* approach. Here, the rotating medium effect enters through a Coriolis force $\boldsymbol{F}_c$ acting on the quasi-particle, resulting in curved trajectory. However, since the Sagnac effect is independent of the medium's refraction index n [13] and so is the rotation induced phase in our Green's function analysis, the *consistent* model of $\boldsymbol{F}_c$ must also be n-independent. Therefore we express it as $F_c = 2\boldsymbol{p}_0 \times \boldsymbol{\Omega}$ where $\boldsymbol{p}_0$ is the *free space* momentum. This force is identical to the rate of change of the quasi-particle actual momentum $\boldsymbol{p}$, that according to Minkowski model is $\boldsymbol{p} = \boldsymbol{p}_0 n$. We arrive at the equation of motion

$$2\boldsymbol{p}_0 \times \boldsymbol{\Omega} = \dot{\boldsymbol{p}}_0 n \tag{10}$$

where the over-dot indicates a time derivative. Hence $\dot{\boldsymbol{p}}_0 = n^{-1} 2\boldsymbol{p}_0 \times \boldsymbol{\Omega}$. This directly implies that the curvature of the quasi-particle trajectory is inversely proportional to n. Thus lower index induces tighter bending.

Summary A concise theory of radiation from point sources embedded in a rotating medium, and observed in its rest-frame, was presented. The formulas developed are easy to employ in any physical system. The formulation was used to illustrate the Sagnac effect as a simplified series of nearest-neighbor scattering events, leading to the known result where the rotation induced phase depends on the area enclosed by the scatterer array, and is medium *independent*. This formulation was then used to treat the problem of diffraction from a linear array of emitters embedded in a rotating medium, giving rise to rotation induced "bending" of the interference pattern. Unlike the Sagnac effect, the bending is medium *dependent* with a curvature inversely proportional to the rotating medium refractive index. Therefore, low-index metamaterials can be used to enhance rotation-induced effects. This result is counter intuitive as one expects that a faster wave would experience weaker bending, and lends itself to interpretations in a dual way. From the calculated fields point of view, the bending is associated with the inverse dependence of the power flux and Abraham momentum on the refractive index. From a quasiparticle-diffraction point of view, we can treat the bending of the fields using the action of an equivalent Coriolis type force, where the Minkowski momentum picture is the appropriate one here, in a manner consistent with the interpretation presented in [37].

Acknowledgement The author BZS gratefully acknowledges fruitful discussions with Prof. Hui Cao at Yale. YM would like to thank Prof. Andrea Alu for his support. This research was supported in part by AFOSR grant# FA9550-18-1-0208.

[1] C. Caloz, A. Alù, S. Tretyakov, D. Sounas, and K. Achouri and Z. L. Deck-Léger, "Electromagnetic Nonreciprocity", *Phys. Rev. Applied*, **10**, 047001 (2018).

[2] Rayleigh, "On the magnetic rotation of light and the second law of thermodynamics", *Nature*, **64**, 577 (1901)

[3] D. M. Pozar, *Microwave engineering*, Wiley (Hoboken (N.J.)), 2012.

[4] M. Trzeciecki and W. Hübner, "Time-reversal symmetry in nonlinear optics," *Phys. Rev. B*, **62**, 13888 (2000).

[5] S. Naguleswaran and G. E. Stedman, "Onsager relations and time-reversal symmetry in nonlinear optics", *J. of Phys. B*, **31**, 935, (1998).

[6] Z. Yu and S. Fan, "Complete Optical Isolation

Created by Indirect Interband Photonic Transitions," *Nat. Photon.* **3**, 91 (2009)

[7] H. Lira, Z. Yu, S. Fan, and M. Lipson, "Electrically Driven Nonreciprocity Induced by Interband Photonic Transition on a Silicon Chip," *Phys. Rev. Lett.* **109**, 033901 (2012).

[8] M. B. Zanjani, A. R. Davoyan, A. M. Mahmoud, N. Engheta, J. R. Lukes, "One-way Phonon Isolation In Acoustic Waveguides," *arXiv*:1312.0082 (2013)

[9] D. L. Sounas, C. Caloz, and A. Al, ' "Giant Non-Reciprocity at the Subwavelength Scale Using Angular Momentum-Biased Metamaterials," *Nat. Communications*, **4**, 2407 , (2013)

[10] D. Sounas, and A. Alu, "Angular-Momentum-Biased Nanorings to Realize Magnetic-Free Integrated Optical Isolation," *ACS Photonics*, **1**, 198-204, (2014)

[11] R. Fleury, D. L. Sounas, C. F. Sieck, M. R. Haberman, and A. Al, "Sound Isolation and Giant Linear Nonreciprocity in a Compact Acoustic Circulator," *Science*, **343**, 516-519, (2014)

[12] S. Lennebere and M. G. Silveirinha, "Wave instabilities and unidirectional light flow in a cavity with rotating walls," *Phys. Rev. A*, **94**, 033810 (2016)

[13] E. J. Post, "Sagnac Effect," *Rev. Mod. Phys.* **39**(2), pp. 475-493, April 1967.

[14] *Fiber-Optic Rotation Sensors*, edited by S. Ezekiel and H. J. Arditty, Springer Series In Optical Sciences (Springer-Verlag, Berlin, 1982).

[15] H. J. Arditty and H. C. Lefevre, "Sagnac effect in fiber gyroscopes," *Opt. Lett.* **6**(8), pp. 401-403, Aug. 1981.

[16] H. C. Lefevre, "Fundamentals of the Interferometric Fiber-Optic Gyroscope," *Opt. Rev.* **4**(1A), pp. 20-27, 1997.

[17] Ben Z. Steinberg, "Rotating Photonic Crystals: A Medium for Compact Optical Gyroscopes," *Phys. Rev. E*, **71**, pp. 056621 1-7, 2005.

[18] Ben Z. Steinberg and A. Boag, "Splitting of Micro-Cavity Degenerate Modes in Rotating Photonic Crystals - The Miniature Optical Gyroscopes," *J. Opt. Soc. Am. B*, **24**(1), pp. 142-151, 2007.

[19] Ben Z. Steinberg, Jacob Scheuer, and A. Boag, "Rotation Induced Super Structure in Slow-Light Waveguides with Mode Degeneracy: Optical Gyroscopes with Exponential Sensitivity," *J. Opt. Soc. Am. B*, **24**(5), pp. 1216-1224, 2007.

[20] J. Scheuer and A. Yariv, "Sagnac effect in coupled resonator slow light waveguide structures," *Phys. Rev. Lett.* **96**, 053901, 2006.

[21] J. Scheuer, "Heavy and Light photon bands induced by symmetry in a linear array of Sagnac reflectors," *Opt. Eng.*, **53**(10), 102707, 2014.

[22] S. Sunada and T. Harayama, "Sagnac effect in resonant microcavities," *Phys. Rev. A*, **74**, 021801(R), 2006.

[23] Li Ge, R. Sarma, and Hui Cau, "Rotation-induced mode coupling in open wavelength-scale microcavities," *Phys. Rev. A*, **90**, 013809, 2014.

[24] R. Sarma, Li Ge, J. Wiersig, and Hui Cao, "Rotating Optical Microcavities with Broken Chiral Symmetry" *Phys. Rev. Lett.*, **114**, 053903, 2015.

[25] T. Shiozawa, "Phenomenological and Electron-Theoretical Study of the Electrodynamics of Rotating Systems," *Proc. IEEE* **61**(12), pp. 1694-1702, Dec. 1973.

[26] J. L. Anderson and J. W. Ryon, "Electromagnetic Radiation in Accelerated Systems," *Physical Review* **181**(5) pp. 1765-1775, 1969.

[27] C. W. Misner, K. S. Thorne, and J. A. Wheeler, *Gravitation*, Princeton University Press, 2017.

[28] R. Sarma, H. Noh, and Hui Cao, "Wavelength-scale microdisks as optical gyroscopes: a finite-difference time-domain simulation study," *J. Opt. Soc. Am. B*, **29**(7), 1648, 2012.

[29] R. Novitski, J. Scheuer, and Ben Z. Steinberg, "Unconditionally stable finite-difference time-domain methods for modeling the Sagnac effect," *Phys. Rev. E*, **87**, 023303, 2013.

[30] J. Van Bladel, "Electromagnetic Fields in the Presence of Rotating Bodies," *Proc. IEEE* **64**(3), pp. 301-318, Mar. 1976.

[31] Daniel De Zutter and D. Goethals, "Scattering by a Rotating Conducting Sphere," *IEEE Trans. Ant. Propag.*, **32**(1), pp. 95-98, Jan. 1984.

[32] Ben Z. Steinberg, A. Shamir, and A. Boag, "Two-dimensional Greens function theory for the electrodynamics of rotating medium," *Phys. Rev. E*, **74**, pp. 016608 1-9, 2006.

[33] Y. Mazor and Ben Z. Steinberg, Supplemental material.

[34] I. Kazma and Ben Z. Steinberg, "Breach of symmetries in rotating arrays and metamaterials observed in their rest frame," URSI EM Theory Symposium, EMTS 2019, San Diego, CA, 2731 May 2019. Available also in http://arxiv.org/abs/1908.05172

[35] U. Leonhardt and P. Piwnicki, "Optics of nonuniformly moving media," *Phys. Rev. A* **60**(6), pp. 4301-4312, Dec. 1999.

[36] T. Ramos, G. F. Rubilar, and Y. N. Obukhov, "First principles approach to the Abraham-Minkowski controversy for the momentum of light in general linear non-dispersive media," *J. Opt.*, **17** 025611, 2015.

[37] Stephen M. Barnett, "Resolution of the Abraham Minkowski Dilema," *Phys. Rev. Lett.*, **104** 070401, 2010.

[38] A. H. Sihvola, A. J. Viitanen, I .V. Lindell, and S. A. Tretyakov *Electromagnetic Waves in Chiral and Bi-Isotropic Media*, Artech House, 1994